

Ground State Properties of the Two-Dimensional t - J Model

M. Kohno

Institute for Solid State Physics,

University of Tokyo, Roppongi, Minato-ku, Tokyo 106

(October 29, 2018)

Abstract

The two-dimensional t - J model in the ground state is investigated by the power Lanczos method. The pairing-pairing correlation function for $d_{x^2-y^2}$ -wave symmetry is enhanced in the realistic parameter regime for high- T_c superconductors. The charge susceptibility χ_c shows divergent behavior as $\chi_c \propto \delta^{-1}$ near half-filling for the doping concentration δ , indicating that the value of the dynamical exponent z is four under the assumption of hyper-scaling. The peak height of the spin structure factor $S_{\max}(Q)$ also behaves as $S_{\max}(Q) \propto \delta^{-1}$ near half-filling, which leads to the divergence of the antiferromagnetic correlation length ξ_m as $\xi_m \propto \delta^{-1/2}$. The boundary of phase separation is estimated on the basis of the Maxwell construction. Numerical results are compared with experimental features observed in high- T_c cuprates.

71.27.+a, 71.10.Fd, 71.30.+h, 75.40.Cx

I. INTRODUCTION

Since the discovery of high- T_c cuprate superconductors [1], many microscopic models have been proposed in order to explain the pairing mechanism. The best way to understand the essential feature of the pairing mechanism would be to find the simplest and realistic model that describes the low-energy properties of the copper-oxide planes. The two-dimensional t - J model is one of the candidates for the effective model for the copper-oxide planes [2,3]. As far as superconductivity is concerned, E. Dagotto and J. Riera have obtained indications of superconductivity by an unbiased diagonalization approach in the region of $J/t \lesssim 3$ near quarter-filling [4]. More investigation is necessary in the realistic region of couplings and densities in order to confirm that the two-dimensional t - J model can really be an effective model for high- T_c superconductors. One of the purposes of this paper is to investigate the relevancy of the two-dimensional t - J model as a low-temperature effective model for high- T_c cuprates.

Also, strong electron correlation in low-dimensional systems is one of the central issues in condensed matter physics. The Mott transition is one of the remarkable consequences of strong correlation. In general, there are two types of the Mott transitions for electron systems [5]. One is characterized by the vanishment of the carrier density, the other is characterized by the divergence of the carrier mass. A typical example which shows the first type of transition is the free-fermion model on a lattice. In this case, the dynamical exponent z is two [6]. A typical example which shows the second type of the Mott transition is the two-dimensional Hubbard model [7,8]. It has been shown numerically that the value of the dynamical exponent z is four in the case of the two-dimensional Hubbard model [6,9]. A naive expectation is that the two-dimensional t - J model shows the same type of the Mott transition as that of the two-dimensional Hubbard model, because the t - J model can be derived as an effective model for the Hubbard model in the limit of $U \rightarrow \infty$. However, in the large J/t regime, the t - J model shows different properties from those of the Hubbard model. For example, if J/t is so large that phase separation occurs, the transition to an

insulator is a first order transition. In the region of J/t slightly smaller than the phase-separation boundary, it is expected that electrons (or holes) form bound states due to the effective attractive forces that lead to phase separation. It is interesting to investigate the critical phenomena toward half-filling in this parameter regime. Hence, in this paper, we investigate the Mott transition of the two-dimensional t - J model in the ground state near half-filling.

Several obstacles to numerical calculations have prevented us from getting the low-energy properties of the two-dimensional t - J model. For example, the system size achieved by the exact diagonalization is restricted to about 26 sites near half-filling. On the other hand, Quantum Monte Carlo algorithms have a serious sign problem. Recent progress of a Green's function Monte Carlo algorithm (power Lanczos method [10]) makes it possible for us to investigate the ground state properties of the t - J model in relatively large systems. In this paper, we use the usual Lanczos algorithm for clusters up to 20 sites and the power Lanczos method for larger clusters.

In Sec. II, the t - J model is defined and the power Lanczos method is briefly reviewed. In Sec. III, we show the ground state energy as a function of filling and discuss phase separation on the basis of the Maxwell construction. In Sec. IV, numerical results on the pairing-pairing correlation function are presented. In Sec. V, the Mott transition at $J/t = 0.5$ in the two-dimensional t - J model is discussed on the basis of the hyperscaling hypothesis. Section VI is devoted to summary.

II. MODEL AND METHOD

The t - J model is defined by the following Hamiltonian:

$$\begin{aligned}
 \mathcal{H}_{tJ} &= \mathcal{H}_t + \mathcal{H}_J, \\
 \mathcal{H}_t &= -t \sum_{\langle i,j \rangle \sigma} (\tilde{c}_{i\sigma}^\dagger \tilde{c}_{j\sigma} + \text{h.c.}), \\
 \mathcal{H}_J &= J \sum_{\langle i,j \rangle} (\mathbf{S}_i \cdot \mathbf{S}_j - \frac{1}{4} n_i n_j),
 \end{aligned} \tag{2.1}$$

where $\tilde{c}_{i\sigma}^\dagger$ denotes a creation operator of an electron at site i with spin σ ($\sigma = \uparrow, \downarrow$) with the constraint that no site is doubly occupied, which is defined as $\tilde{c}_{i\sigma}^\dagger \equiv (1 - n_{i-\sigma})c_{i\sigma}^\dagger$. The number operator $n_{i\sigma}$ is defined as $n_{i\sigma} \equiv c_{i\sigma}^\dagger c_{i\sigma}$, using the standard electron creation operator $c_{i\sigma}^\dagger$. The spin operator at site i is defined as $\mathbf{S}_i \equiv \frac{1}{2} \sum_{\alpha\beta} c_{i\alpha}^\dagger \boldsymbol{\sigma}_{\alpha\beta} c_{i\beta}$, where $\boldsymbol{\sigma}_{\alpha\beta}$ is the vector of Pauli matrices. The summation ($\sum_{\langle i,j \rangle}$) is taken over all nearest neighbor sites on a square lattice.

We adopt the power Lanczos method proposed by Y.C. Chen and T.K. Lee [10]. In the framework of this method, the expectation value of an operator \mathcal{O} in the ground state of a Hamiltonian \mathcal{H} is evaluated by the following equation:

$$\langle \mathcal{O} \rangle = \lim_{p \rightarrow \infty} \langle p\text{L1} | \mathcal{O} | p\text{L1} \rangle / \lim_{p' \rightarrow \infty} \langle p'\text{L1} | p'\text{L1} \rangle, \quad (2.2)$$

where $|p\text{L1}\rangle$ is the wavefunction defined as $|p\text{L1}\rangle \equiv \mathcal{H}^p | \text{L1} \rangle$. The wavefunction $| \text{L1} \rangle$ is defined as $| \text{L1} \rangle \equiv | \text{trial} \rangle + c_1 \mathcal{H} | \text{trial} \rangle$, where $| \text{trial} \rangle$ is a trial wavefunction and c_1 is a variational parameter. if we set $c_1 = 0$, the power Lanczos method reduces to the power method.

The variational wavefunction proposed by R. Valenti and C. Gros [11] is employed as the trial wavefunction:

$$| \phi \rangle = \prod_{ij} | r_i - r_j |^\nu P_G P_N | d\text{-wave} \rangle, \quad (2.3)$$

where ν is a variational parameter and r_i represents the real-space coordinate at site i . The Gutzwiller and N -particle projection operators are denoted by P_G and P_N , respectively. The wavefunction $| d\text{-wave} \rangle$ represents the BCS-wavefunction in which the order parameter has $d_{x^2-y^2}$ -wave symmetry. It should be noted that the trial wavefunction is in the subspace that both the total spin S and the total momentum P are zero. Therefore the ground state properties reported in this paper are within this subspace.

One of the reasons why we use the above wavefunction $| \phi \rangle$ as a trial wavefunction is that this wavefunction gives the lowest energy among variational wavefunctions proposed so far, as far as we know, in the parameter regime we investigated. Another reason is that we can restrict the Hilbert space of simulation within the subspace of $S = 0$ and $P = 0$. This

makes convergence faster. The applicability of the power Lanczos method depends on the negative-sign ratio r which is defined by $r \equiv (p - n)/(p + n)$, where p and n denote the number of positive and negative samples, respectively. If the ratio r is less than 0.1, it is difficult to obtain reliable results. As a result, the applicability of the power Lanczos method is restricted to the power $p < p_r$, where p_r denotes the power at which the ratio r is about 0.1. If the power required to reach convergence (p_c) is larger than p_r , the power Lanczos method is not applicable. If we use a wavefunction which has small overlap with the ground-state wavefunction, it requires large power to reach the ground state. We compare the speed of convergence of the power Lanczos method and the simple power method using the Gutzwiller wavefunction and $|\phi\rangle$ as a trial wavefunction. As shown in Fig.1, the power Lanczos method requires smaller power p than the simple power method, and the wavefunction $|\phi\rangle$ is superior to the Gutzwiller wavefunction as a trial wavefunction. In this figure, the error in energy due to finite power p is less than 0.2% for $p > 5$ by the power Lanczos method using $|\phi\rangle$, although p_c becomes larger than p_r if we use the Gutzwiller wavefunction.

We have checked convergent behavior in each simulation using $|\phi\rangle$ as a trial wavefunction. The p_c becomes larger, if the system size becomes larger. For 50-site clusters, p_c is about eight for the energy to converge. The p_r becomes smaller, if J gets smaller. The most severe p_r in our simulation is about eight near half-filling for $J \simeq 0.3$. As an example, we show the convergence of energy in a 50-site cluster with 42 electrons at $J = 0.3$ in Fig.2. We measure physical quantities at $p \simeq 8$, where we have checked in each simulation that the energy converges within a required accuracy. As a check of convergence of physical quantities, we show the pairing-pairing correlation function in a 20-site cluster with 18 electrons at $p = 8$ in Fig.3.

In the following sections, we show the numerical results in finite-size clusters up to 104 sites. The boundary conditions are chosen for the momentum configuration to be closed-shell. We have typically run 1000-2000 Monte Carlo steps. Several hundred branches are produced at each Monte Carlo step in the evaluation of powers of \mathcal{H} .

The filling n is defined as $n \equiv N_e/N_s$, where N_e is the number of electrons and N_s is

the number of sites. The doping concentration δ is defined as $\delta \equiv 1 - n$. The ground state energy per site at filling n is denoted by $e(n)$. Hereafter we set $t = 1$ as the energy unit.

III. PHASE SEPARATION

Before investigating phase separation of the two-dimensional t - J model, we examine the finite-size effects on the ground state energy in the free-fermion model on a square lattice, in which we can calculate the exact ground state energy with any size of systems. We calculate the ground state energy per site of the free-fermion model in the same system sizes under the same boundary conditions as those used in the t - J model. We fit them as a function of filling by a polynomial up to third order. As shown in Fig.4, the fitting curve (dotted line) almost coincides with the curve in the thermodynamic limit (solid line). The finite-size effects on the ground state energy of the two-dimensional t - J model is probably not so different from those of the free-fermion model on a square lattice. Actually, as shown in Fig.5, the data of the ground state energy per site of the two-dimensional t - J model in finite-size clusters are well fitted by a polynomial as a function of filling with small deviation from the fit, indicating that the finite-size effects on the ground state energy are small.

Figure 5 shows the ground state energy per site as a function of filling in the two-dimensional t - J model at $J = 0.5, 1.0, 1.5, 2.0, 2.5$ and 3.0 . In this figure, the tangent from the point at $n = 1$ to the fitting curve gives a lower energy than the fitting curve in the region of $n_c < n < 1$ as represented by the solid line. Here n_c is the electron density at the point of contact between the fitting curve and the tangent. Hence, we can identify the region of phase separation as $n_c < n < 1$ on the basis of the Maxwell construction [12]. The energy and the chemical potential of the phase-separated state are given as the tangent and its slope, respectively. At $J = 3.5$, we find that the critical density n_c is zero. On the other hand, as shown in Fig.8, the chemical potential at $J = 0.5$ shows a monotonically increasing behavior as a function of filling at least in the region of $n \gtrsim 0.95$, indicating that phase separation does not occur at $J = 0.5$. Hence, the phase-separation boundary is obtained as

in Fig.12. The critical J above which no stable homogeneous state exists is estimated as $J_{c_1} = 3.4 \pm 0.1$. The critical J below which no phase-separated state exists is estimated as $J_{c_2} = 0.75 \pm 0.25$.

The critical value of J_{c_1} is obtained more accurately in Ref.13 as 3.4367 ± 0.0001 by solving the equation of motion of two electrons. The numerical result in this paper is consistent with it. The estimation of J_{c_2} is consistent with that in Ref.14 ($J_{c_2} \simeq 0.75$). In the intermediate region of n , the phase-separation boundary estimated in this paper is qualitatively similar to those in Ref.4 or Ref.15, but quantitatively lower than them (Fig.12).

In the following sections, we show the numerical results at $J = 0.5$. At this J , phase separation does not occur as discussed in this section.

IV. PAIRING-PAIRING CORRELATION

In this section, we show numerical results on the pairing-pairing correlation functions $P_{\pm}(r)$ defined as

$$P_{\pm}(r) \equiv \frac{1}{N_s} \sum_{r_0} \langle \Delta_{\pm}(r_0)^{\dagger} \Delta_{\pm}(r_0 + r) \rangle. \quad (4.1)$$

Here, the singlet pairing operators $\Delta_{\pm}(r)$ are defined as $\Delta(r) \equiv c_{r\uparrow}(c_{r+\hat{x}\downarrow} + c_{r-\hat{x}\downarrow} \pm c_{r+\hat{y}\downarrow} \pm c_{r-\hat{y}\downarrow})$, where $+$ and $-$ correspond to extended s -wave and $d_{x^2-y^2}$ -wave symmetry, respectively and the unit vectors in x - and y - directions are represented by \hat{x} and \hat{y} , respectively.

In Fig. 6(b), the pairing-pairing correlation function with $d_{x^2-y^2}$ -wave symmetry decays very little for $n = 0.84$, although the pairing-pairing correlation function with $d_{x^2-y^2}$ -wave symmetry quickly decays for $n = 0.20$ as shown in Fig. 6(a).

We define here the reduced pairing susceptibility as

$$\tilde{\chi}_{\pm}^P \equiv \sum_{|r|>2} P_{\pm}(r). \quad (4.2)$$

Figures 7 (a) and (b) show the filling-dependence of $\tilde{\chi}_{\pm}^P/\tilde{N}_s$, where \tilde{N}_s is defined as $\tilde{N}_s \equiv \sum_{|r|>2} 1$. If the superconducting long-range order exists, the value of $\tilde{\chi}_{\pm}^P/\tilde{N}_s$ remains finite in

the thermodynamic limit. In Figs.7 (a) and (b), the pairing-pairing correlation for $d_{x^2-y^2}$ -wave symmetry is enhanced in the region of $0.6 \lesssim n \lesssim 1$, and that for extended s -wave symmetry is a little enhanced in the low-density regime.

The numerical results showing that the $d_{x^2-y^2}$ -wave component of the pairing-pairing correlation is dominant near half-filling are consistent with experimental indications, for example, the measurements of the phase coherence in bimetallic YBCO-Pb dc SQUIDS [16].

V. MOTT TRANSITION

In Fig. 8, the filling-dependence for the chemical potential at $J = 0.5$ is shown. The data of the chemical potential in finite-size clusters are calculated as follows:

$$\bar{\mu}(\bar{n}) \equiv \frac{e(n_1) - e(n_2)}{n_1 - n_2}, \quad (5.1)$$

where \bar{n} is taken as $\bar{n} = (n_1 + n_2)/2$. Here, n_1 and n_2 are taken to be adjacent closed-shell filling with boundary conditions fixed. Here, boundary conditions at half-filling are regarded as those under which the momentum configurations are closed-shell in the free-fermion model on a square lattice. In the thermodynamic limit, this definition of the chemical potential reduces to the normal one: $\mu(n) \equiv \partial e(n)/\partial n$.

We fit the data near half-filling in Fig.8(c) as $\mu - \mu_c \propto \delta^\alpha$ and estimate $\mu_c = 1.31 \pm 0.03$ and $\alpha = 1.78 \pm 0.29$, which is close to $\alpha = 2$ reported in the case of the two-dimensional Hubbard model at $U = 4$ [7]. This suggests that the charge susceptibility χ_c defined by $\chi_c \equiv \partial n/\partial \mu$ diverges as $\chi_c \propto \delta^{-1}$ toward half-filling. Actually the chemical potential is fitted well by the following form:

$$|\mu - \mu_c| \propto \delta^2, \quad (5.2)$$

as denoted by the dashed line in Fig.8(a) and (b). In order to check this divergent behavior of the charge susceptibility, we also investigate the doping dependence of chemical potential for $J = 0.3$ and $J = 0.4$. Figure 9 shows the same plot as in Fig.8 for $J = 0.3$ and $J = 0.4$.

From the fit of the numerical data in Fig.9(c), we estimate $\mu_c = 1.88 \pm 0.03$, $\alpha = 1.83 \pm 0.17$ for $J = 0.3$ and $\mu_c = 1.57 \pm 0.02$, $\alpha = 1.98 \pm 0.07$ for $J = 0.4$. The numerical results for $J = 0.3$ and $J = 0.4$ also suggest that the charge susceptibility χ_c diverges as $\chi_c \propto \delta^{-1}$. The divergent behavior of the charge susceptibility is consistent with recent photo-emission measurements [17].

If the hyperscaling relations are satisfied, the charge susceptibility χ_c near the transition point to an insulator is written as $\chi_c \propto \delta^{-(z-d)/d}$, where z is the dynamical exponent and d is the spatial dimensionality [6]. Therefore the numerical results suggest that the value of the dynamical exponent z is four.

We define the spin structure factor $S(k)$ as

$$S(k) \equiv \frac{1}{3} \sum_r \langle \mathbf{S}_0 \cdot \mathbf{S}_r \rangle e^{ikr}. \quad (5.3)$$

Figure 10(a) shows the peak height of the spin structure factor $S_{\max}(Q)$ as a function of filling. The data near half-filling can be fitted well by the following form:

$$S_{\max}(Q) \propto \delta^{-1}, \quad (5.4)$$

as denoted by the dashed line(Fig.10(a), (b) and (c)). We fit the data near half-filling as $S_{\max}(Q)^{-1} \propto \delta^\beta$ and estimate $\beta = 1.02 \pm 0.02$. This suggests that the antiferromagnetic correlation length ξ_m diverges toward half-filling as

$$\xi_m \propto \delta^{-1/2}, \quad (5.5)$$

under the assumption that the spin-spin correlation behaves as $\langle \mathbf{S}_0 \cdot \mathbf{S}_r \rangle \propto e^{iQr} \cdot e^{-r/\xi_m}$ [7]. This behavior of the correlation length has been reported on the two-dimensional Hubbard model at $U = 4$ [7] and is consistent with the observation by neutron scattering experiments [18].

Under the assumption of the existence of the single characteristic length scale ξ that is related to critical phenomena, the hyperscaling theory has predicted that the length scale ξ diverges as $\xi \propto \delta^{-1/d}$ toward the critical point, where d is the spatial dimensionality [6].

The numerical results shown above support the scaling hypothesis and suggest that the Mott transition in the two-dimensional t - J model at $J = 0.5$ is characterized by the dynamical exponent $z = 4$, which is the same as in the case of the two-dimensional Hubbard model at $U = 4$ [6,9].

VI. SUMMARY

Numerical results presented in this paper are consistent with the following experimental features found in the high- T_c oxides: (i) the $d_{x^2-y^2}$ -wave symmetry of the superconducting order parameter in the region of moderate doping, which is suggested by the measurements of the phase coherence in bimetallic YBCO-Pb dc SQUIDS [16] (Sec. IV), (ii) the doping dependence of the antiferromagnetic correlation length near half-filling ($\xi_m \propto \delta^{-1/2}$) observed in neutron scattering experiments [18] (Sec. V), (iii) the large Fermi surface behavior in the region of moderate doping [19] (Fig.11) and (iv) divergent behavior of the charge susceptibility suggested by photo-emission experiments [17] (Sec. V).

In summary, numerical results on the two-dimensional t - J model have been reported. The boundary of phase separation is estimated on the basis of the Maxwell construction (Fig.12). The pairing-pairing correlation for $d_{x^2-y^2}$ -wave symmetry is enhanced in the region of $0.6 \lesssim n \lesssim 1$ at $J = 0.5$ (Fig.7). The charge susceptibility χ_c shows divergent behavior as $\chi_c \propto \delta^{-1}$ toward half-filling, indicating that the value of the dynamical exponent z is four (Figs.8 and 9). The peak height of the spin structure factor $S_{\max}(Q)$ diverges toward half-filling as $S_{\max}(Q) \propto \delta^{-1}$ (Fig.10). This leads to the divergence of the antiferromagnetic correlation length as $\xi_m \propto \delta^{-1/2}$.

ACKNOWLEDGMENTS

The author would like to thank F.F. Assaad, F.V. Kusmartsev, M. Imada, M. Takahashi, N. Furukawa and K. Kusakabe for helpful discussions and useful comments. The author also thanks T. Kawarabayashi and E. Williams for reading of the manuscript. The author would

like to thank A. Ino for sending me the experimental data for the charge susceptibility. The exact diagonalization program is partly based on the subroutine package "TITPACK Ver.2" coded by H. Nishimori and partly on the subroutines coded by K. Kusakabe. Part of the exact diagonalization calculations were performed on the Fujitsu VPP500 of the Supercomputer Center of the Institute for Solid State Physics, Univ. of Tokyo. Part of the Monte Carlo calculations were carried out on the Intel Japan PARAGON at the Institute for Solid State Physics, Univ. of Tokyo.

REFERENCES

- [1] J.G. Bednorz and K.A. Müller, Z. Phys. B **64**, 189 (1986); C.W. Chu, P.H. Hor, R.L. Meng, L. Gao, Z.J. Huang and Y.Q. Wang, Phys. Rev. Lett. **58**, 405 (1987).
- [2] P.W. Anderson, Science **235**, 1196 (1987).
- [3] F.C. Zhang and T.M. Rice, Phys. Rev. B **37**, 3759 (1988).
- [4] E. Dagotto and J. Riera, Phys. Rev. Lett. **70**, 682 (1993).
- [5] M. Imada, J. Phys. Soc. Jpn. **62**, 1105 (1993); M. Imada, J. Phys. Soc. Jpn. **63**, 3059 (1994).
- [6] M. Imada, J. Phys. Soc. Jpn. **64**, 2954 (1995).
- [7] N. Furukawa and M. Imada, J. Phys. Soc. Jpn. **61**, 3331 (1992).
- [8] F.F. Assaad and M. Imada, Phys. Rev. Lett. **74**, 3868 (1995).
- [9] F.F. Assaad and M. Imada, Phys. Rev. Lett. **76**, 3176 (1996).
- [10] Y.C. Chen and T.K. Lee, Phys. Rev. B **51**, 6723 (1995).
- [11] R. Valenti and C. Gros, Phys. Rev. Lett. **68**, 2402 (1992);
C. Gros, Phys. Rev. B **38**, 931 (1988).
- [12] The finite-size effects on the energy in the phase-separated state may be much larger than those in a homogeneous state because of macroscopic fluctuations. The system sizes examined in this paper may be insufficient to obtain an accurate value for the energy of the phase-separated state. Therefore we use the Maxwell construction to determine it.
- [13] C.S. Hellberg and E. Manousakis, Phys. Rev. B **52**, 4639 (1995).
- [14] D. Poilblanc, Phys. Rev. B **52**, 9201 (1995).
- [15] W.O. Putikka, M.U. Luchini and T.M. Rice, Phys. Rev. Lett. **68**, 538 (1992).

- [16] D.A. Wollman, D.J. Van Harlingen, W.C. Lee, D.M. Ginsberg and A.J. Leggett, Phys. Rev. Lett. **71**, 2134 (1993).
- [17] Private communication.
- [18] R.J. Birgeneau, D.R. Gabbe, H.P. Janssen, M.A. Kastner, P.J. Picone, T.R. Thurston, G. Shirane, Y. Endoh, M. Sato, K. Yamada, Y. Hidaka, M. Oda, Y. Enomoto, M. Suzuki and T. Murakami, Phys. Rev. B **38**, 6614 (1988).
- [19] C.G. Olson, *et al.*, Phys. Rev. B **42**, 381 (1990).
- [20] M. Boninsegni and E. Manousakis, Phys. Rev. B **47**, 11897 (1993).
- [21] W.O. Putikka, M.U. Luchini and M. Ogata, Phys. Rev. Lett. **69**, 2288 (1992).

FIGURES

FIG. 1. Energy per site as a function of power p for the 20-site system with 18 electrons at $J = 0.5$. The percentage of the error from the ground state energy corresponds to the vertical scale on the right. Open circles and open diamonds denote the data obtained by the power method and the power Lanczos method, respectively, using the Gutzwiller wavefunction as a trial wavefunction. Solid symbols denote the data by using $|\phi\rangle$ as a trial wavefunction.

FIG. 2. The same plot as in Fig.1 but for the 50-site system with 42 electrons at $J = 0.3$. Inset shows the negative-sign ratio r defined in the text. The dashed line represents $r = 0.1$.

FIG. 3. Pairing-pairing correlation function for $d_{x^2-y^2}$ -wave symmetry in a 20-site cluster with 18 electrons at $J = 0.5$. Crosses denote the data by $|\phi\rangle$ without the power method. Solid diamonds denote the data by the power Lanczos method at $p = 8$, using $|\phi\rangle$ as a trial wavefunction. Open circles denote the exact data obtained by the exact diagonalization.

FIG. 4. Ground state energy per site as a function of filling in the two-dimensional free-fermion model on a square lattice. Dotted line denotes a polynomial fit. Solid line denotes the ground state energy per site in the thermodynamic limit.

FIG. 5. Ground state energy per site as a function of filling in the two-dimensional t - J model at $J = 0.5, 1.0, 1.5, 2.0, 2.5$ and 3.0 , starting from above. Dotted line denotes the same fit as in Fig.4, using data points from $n = 0$ to $n \simeq 0.7$. Solid line denotes the expected ground state energy per site of the phase-separated state which is determined on the basis of the Maxwell construction. Dashed line at $J = 0.5$ is obtained by integrating the fit (dashed line) in Fig.8.

FIG. 6. Pairing-pairing correlation function as a function of distance for (a) $n = 0.20$ and (b) $n = 0.84$ at $J = 0.5$ in 50-site clusters. Crosses and solid diamonds denote the pairing-pairing correlation functions for extended s -wave symmetry and $d_{x^2-y^2}$ -wave symmetry, respectively.

FIG. 7. Reduced pairing susceptibility per site ($\tilde{\chi}_{\pm}^P/\tilde{N}_s$) as a function of filling at $J = 0.5$ for (a) extended s -wave symmetry and (b) $d_{x^2-y^2}$ -wave symmetry, where $\tilde{\chi}_{\pm}^P \equiv \sum_{|r|>2} P_{\pm}(r)$ and $\tilde{N}_s \equiv \sum_{|r|>2} 1$.

FIG. 8. Chemical potential as a function of filling at $J = 0.5$, (a) linear plot, (b) μ vs δ^2 plot and (c) log-log plot. Dotted line in (a) and (b) is obtained by differentiating the fit at $J = 0.5$ (dotted line) in Fig.5. Dashed line in (a) and (b) denotes a fit as $|\mu - \mu_c| \propto \delta^2$. Dashed and solid lines in (c) correspond to the cases of the dynamical exponent $z = 2$ and $z = 4$, respectively.

FIG. 9. Chemical potential as a function of filling at $J = 0.3, 0.4$ and 0.5 starting from above, (a) linear plot, (b) μ vs δ^2 plot. (c) Log-log plot for $J = 0.3$ (open symbols) and $J = 0.4$ (solid symbols). Dashed line in (a) and (b) denotes a fit as $|\mu - \mu_c| \propto \delta^2$. The point denoted by a cross is obtained by a Green's function Monte Carlo in a 10×10 -site cluster with two holes taken from Ref.20. Dashed and solid lines in (c) correspond to the cases of the dynamical exponent $z = 2$ and $z = 4$, respectively.

FIG. 10. Peak height of the spin structure factor $S_{\max}(Q)$ as a function of filling at $J = 0.5$, (a) linear plot, (b) $S_{\max}(Q)^{-1}$ vs δ plot and (c) log-log plot. Dashed line in (a), (b) and (c) denotes a fit in the form of $S_{\max}(Q) \propto \delta^{-1}$.

FIG. 11. Momentum distribution function for $n = 0.84$ at $J = 0.5$ in a 50-site cluster. In the inset, solid and dashed lines denote the Fermi Surface and the Brillouin zone boundary, respectively. The center is the Γ -point.

FIG. 12. Schematic phase diagram of the two-dimensional t - J model in the ground state. Solid diamonds denote the phase-separation boundary obtained in Sec. III. In the higher-density region than the open diamond, the pairing-pairing correlation for $d_{x^2-y^2}$ -wave symmetry is enhanced. It should be noted that a ferromagnetic phase may exist in the small J region ($J \lesssim 0.1$) suggested in Refs.15 and 21. This ferromagnetic phase is beyond the scope of this paper.

Fig.1 M.Kohno

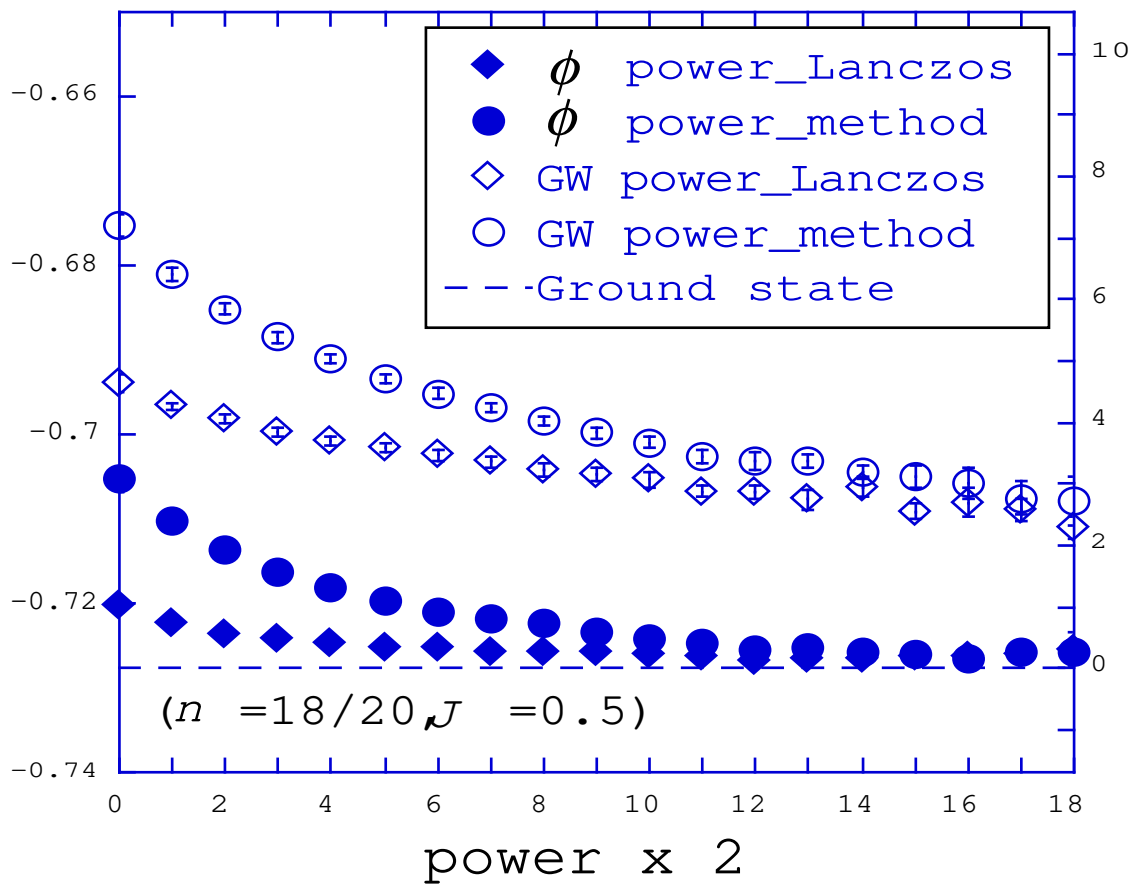


Fig.2 M.Kohno

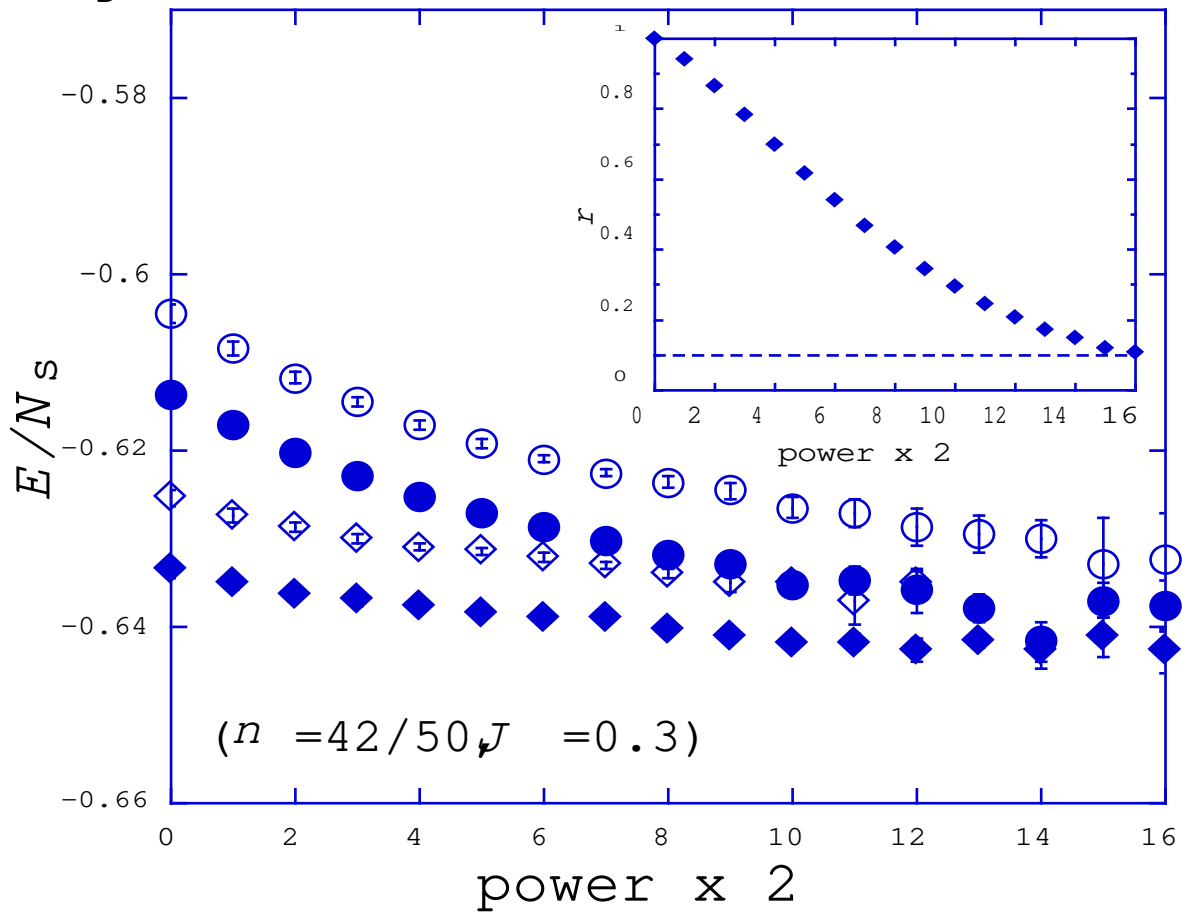


Fig. 6 (a)

M. Kohno

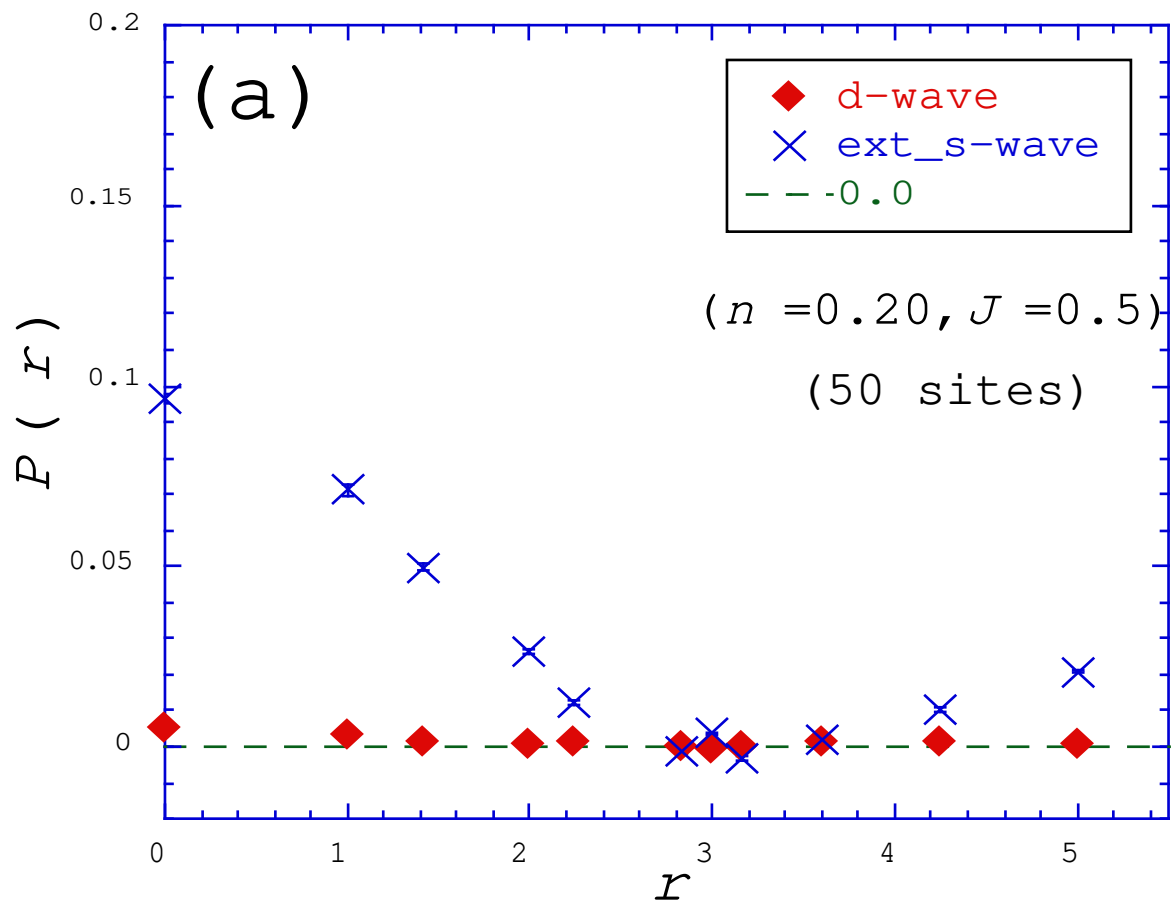


Fig. 6 (b)

M. Kohno

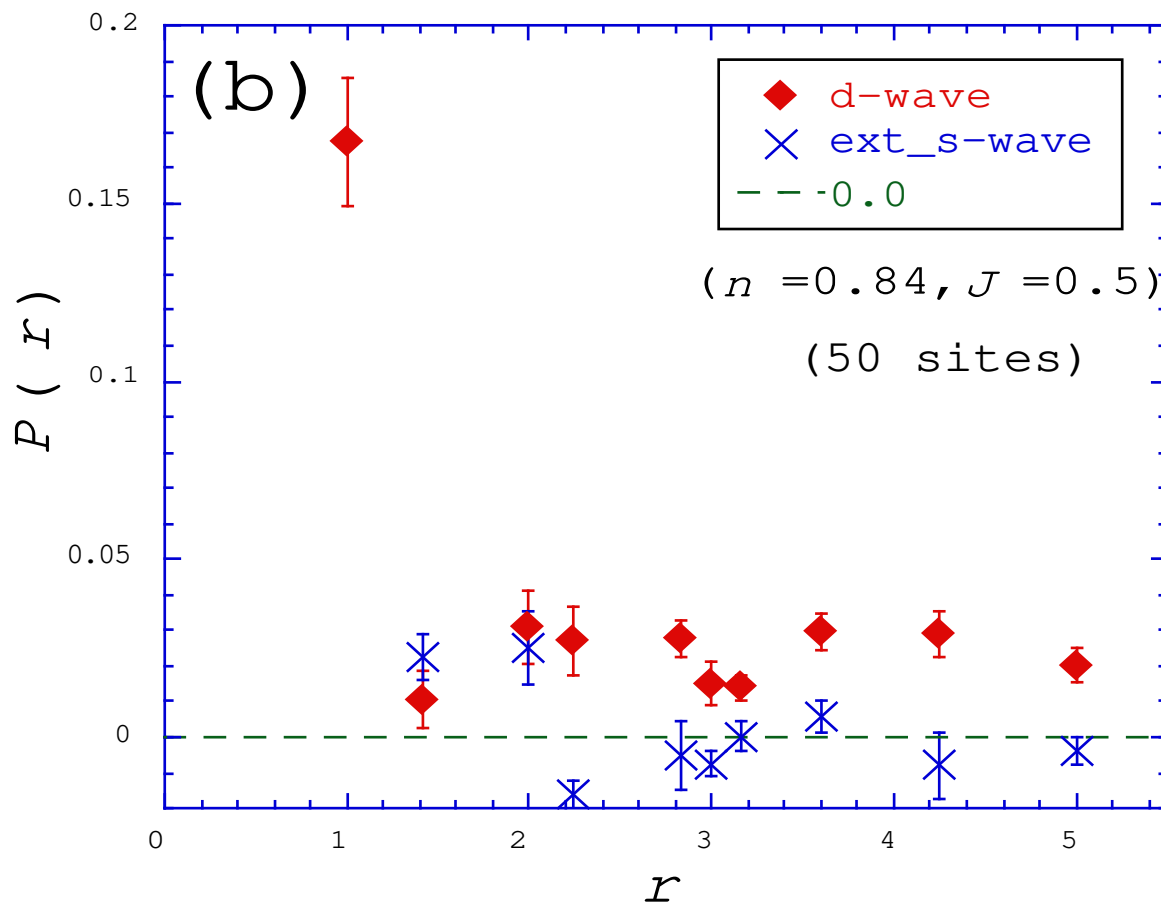


Fig. 7 (a) M. Kohno

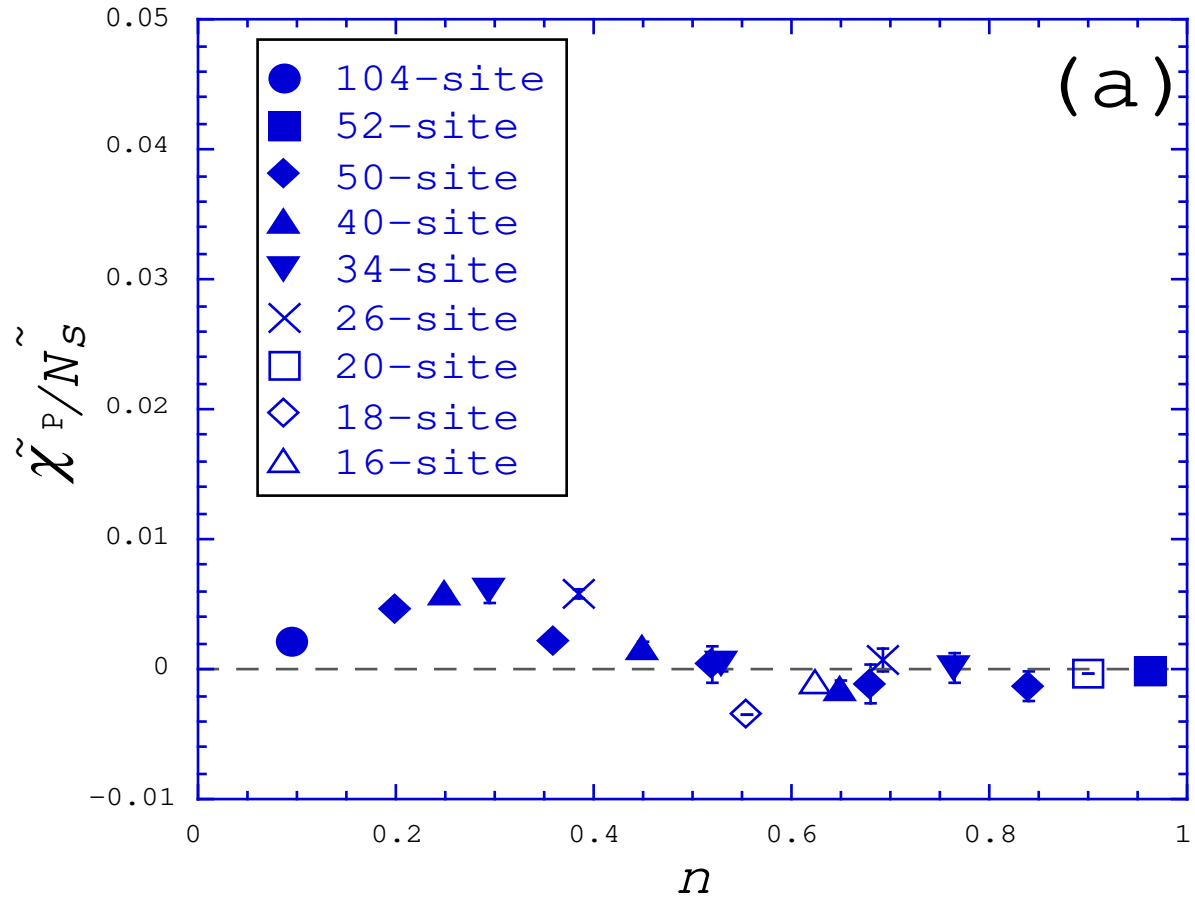


Fig. 7 (b) M. Kohno

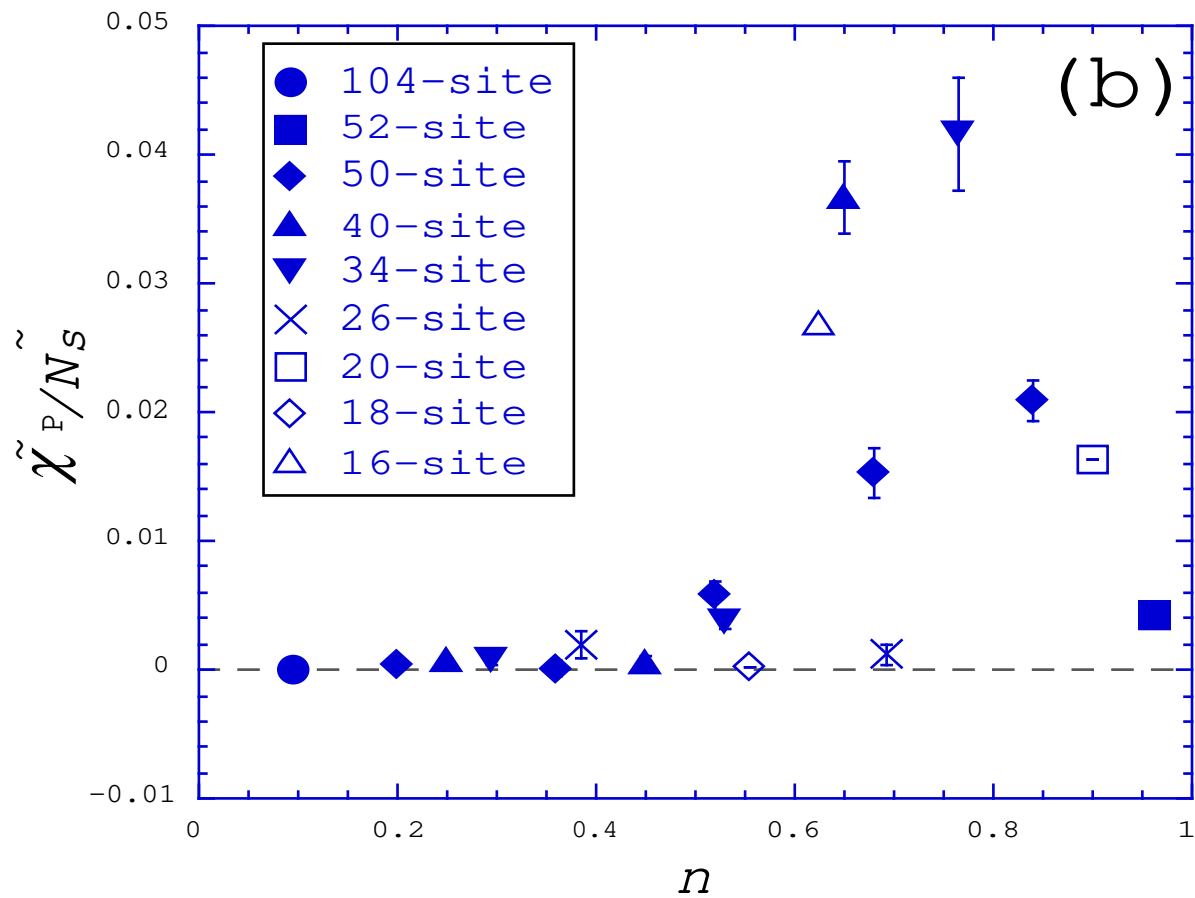


Fig. 8 (a)

M.Kohno

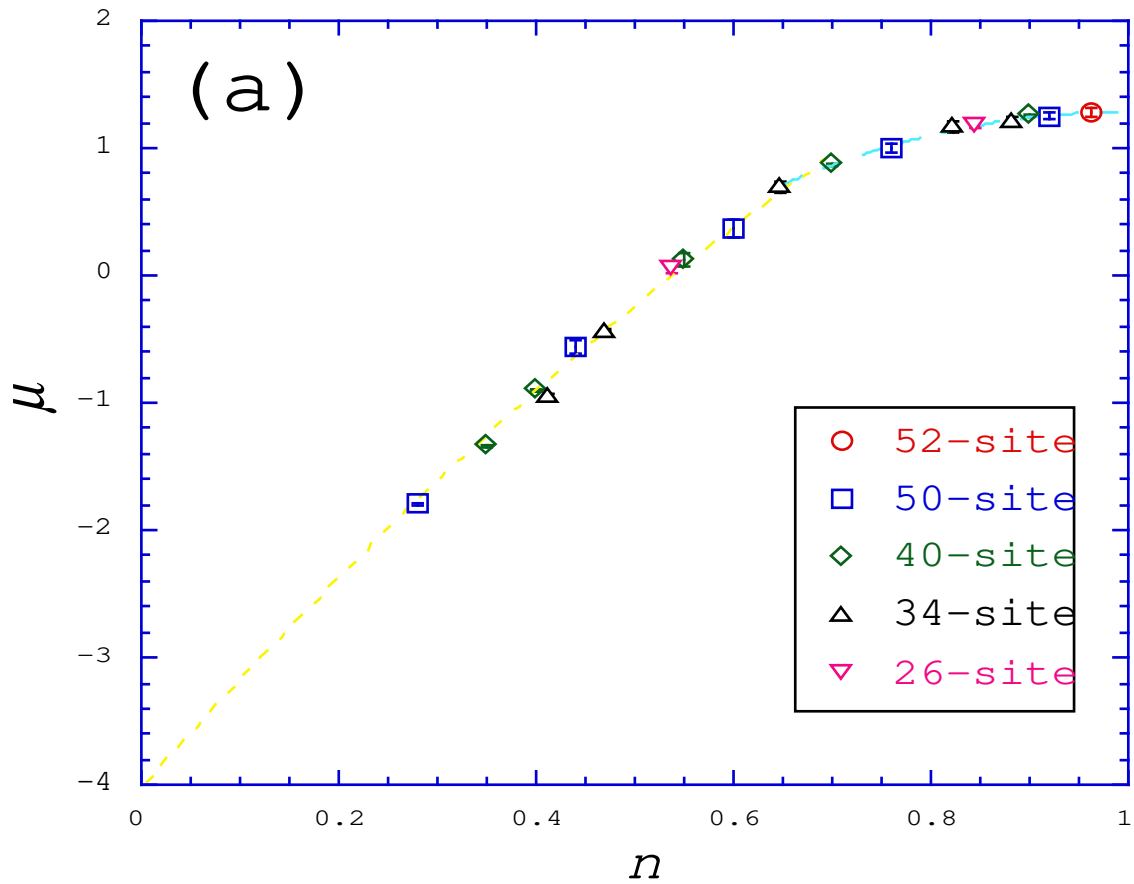


Fig. 8 (b)

M.Kohno

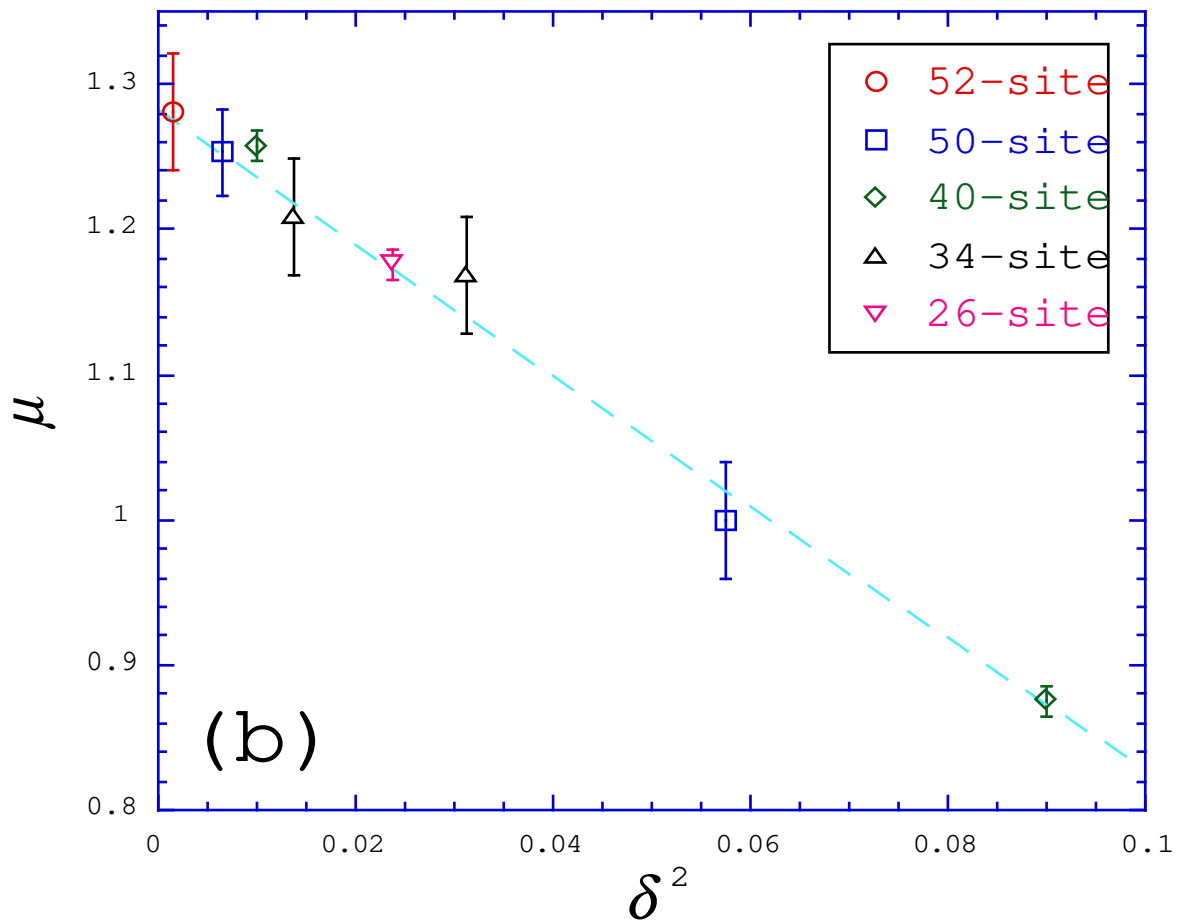


Fig. 8 (c)

M. Kohno

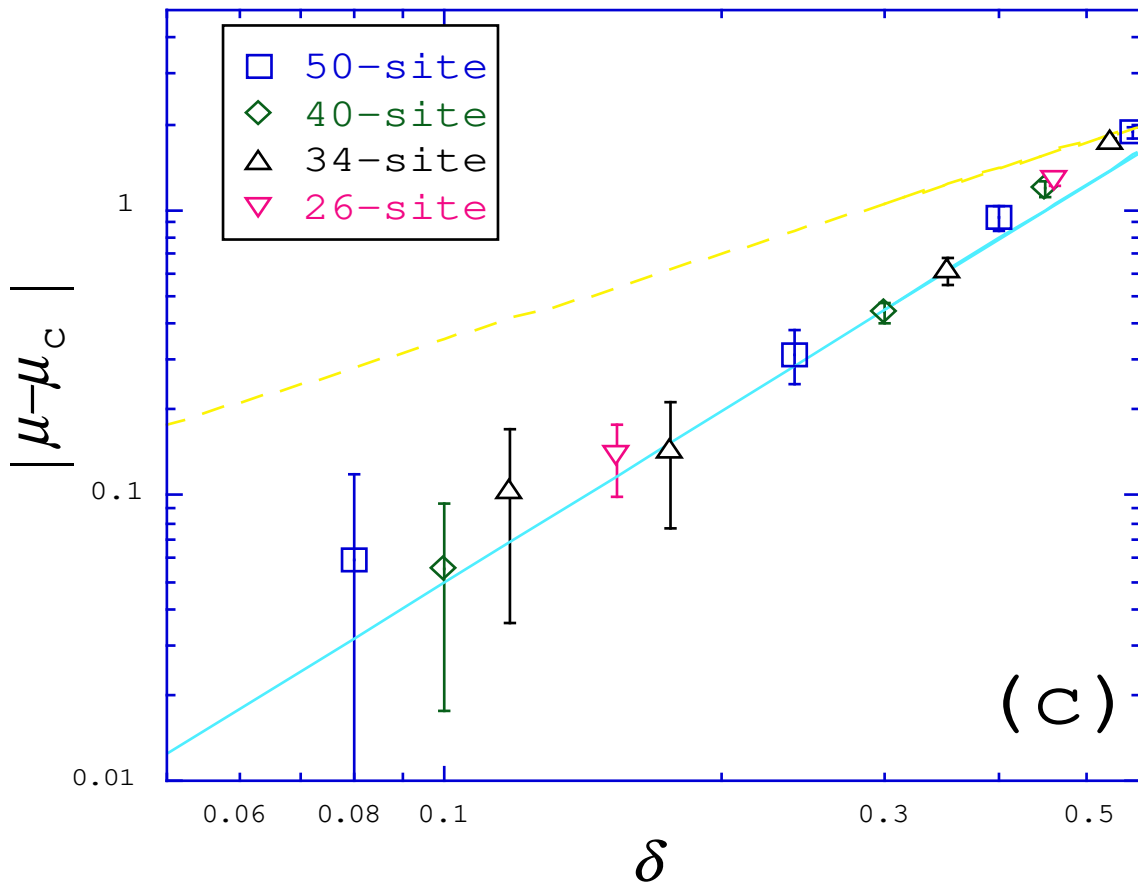


Fig. 9 (a)

M. Kohno

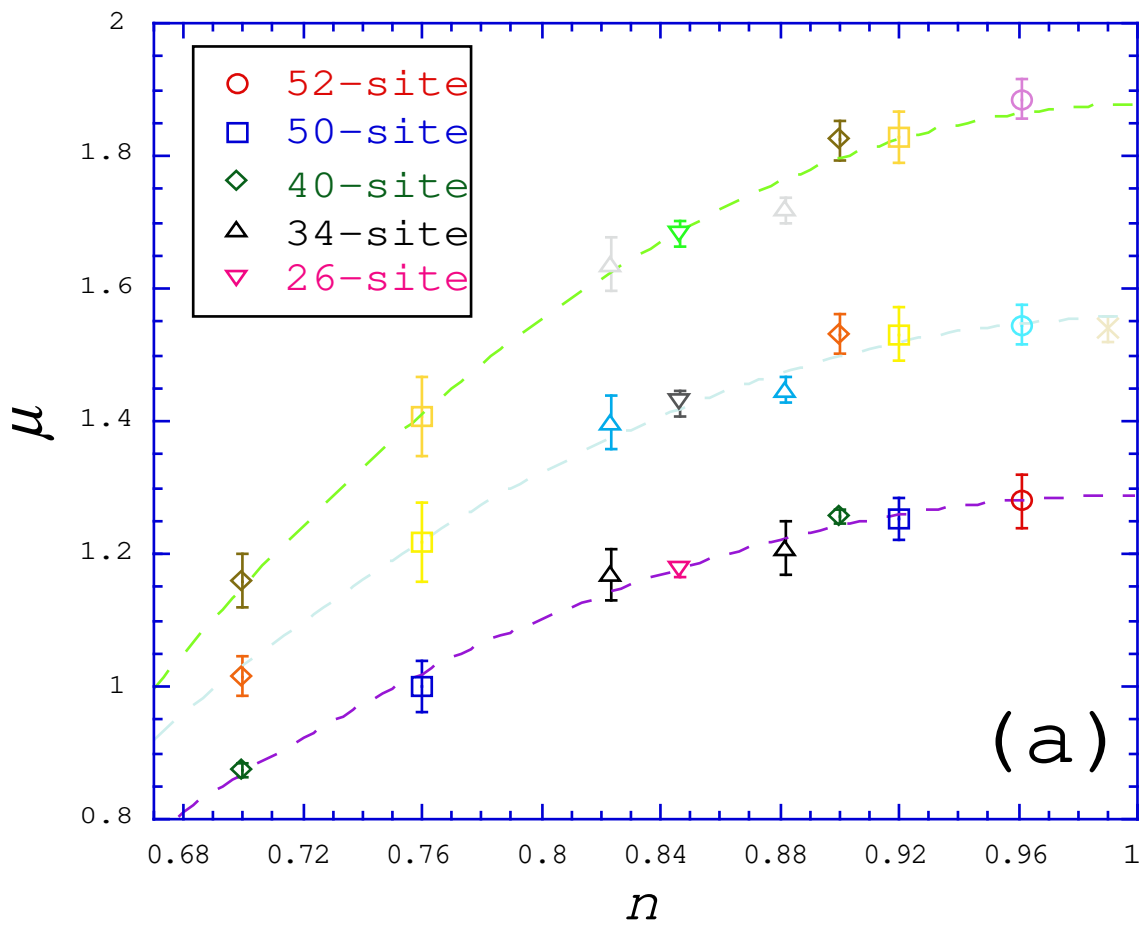


Fig. 9 (b) M. Kohno

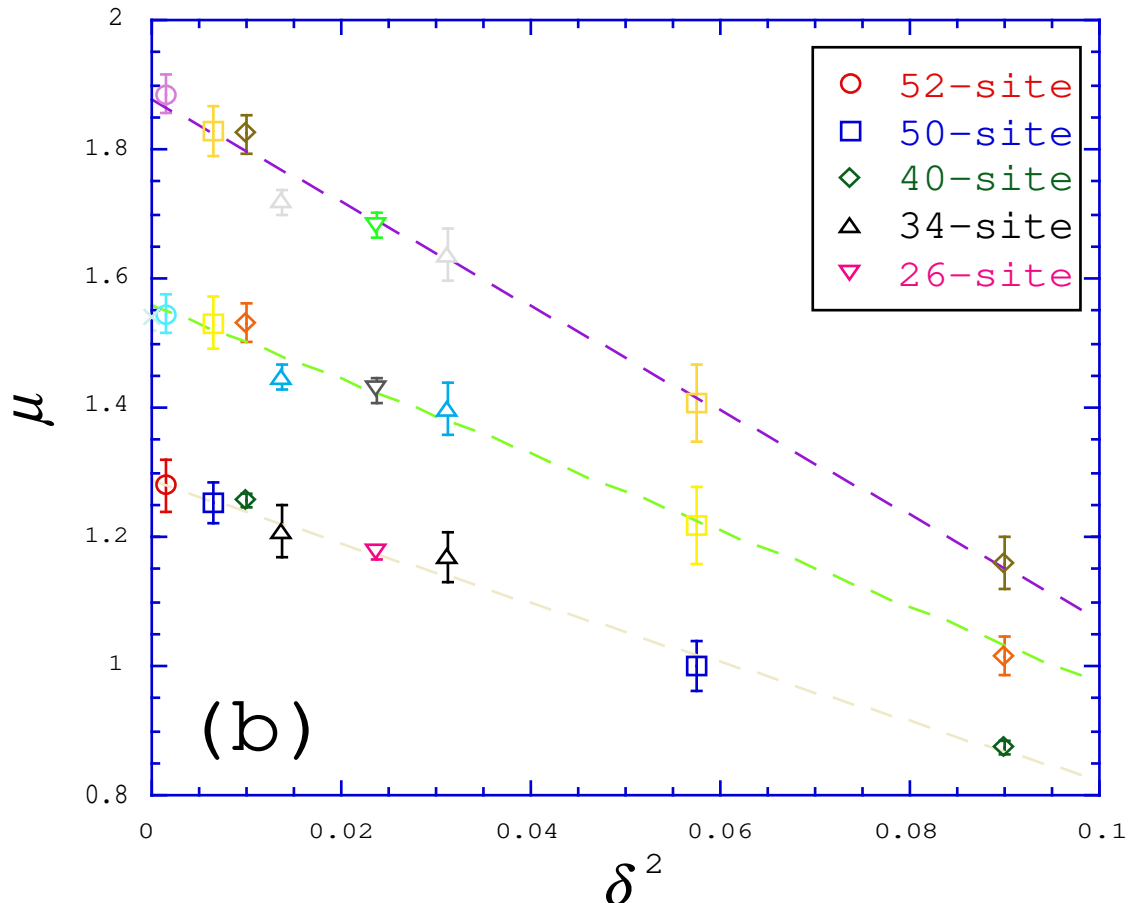


Fig. 9 (c) M. Kohno

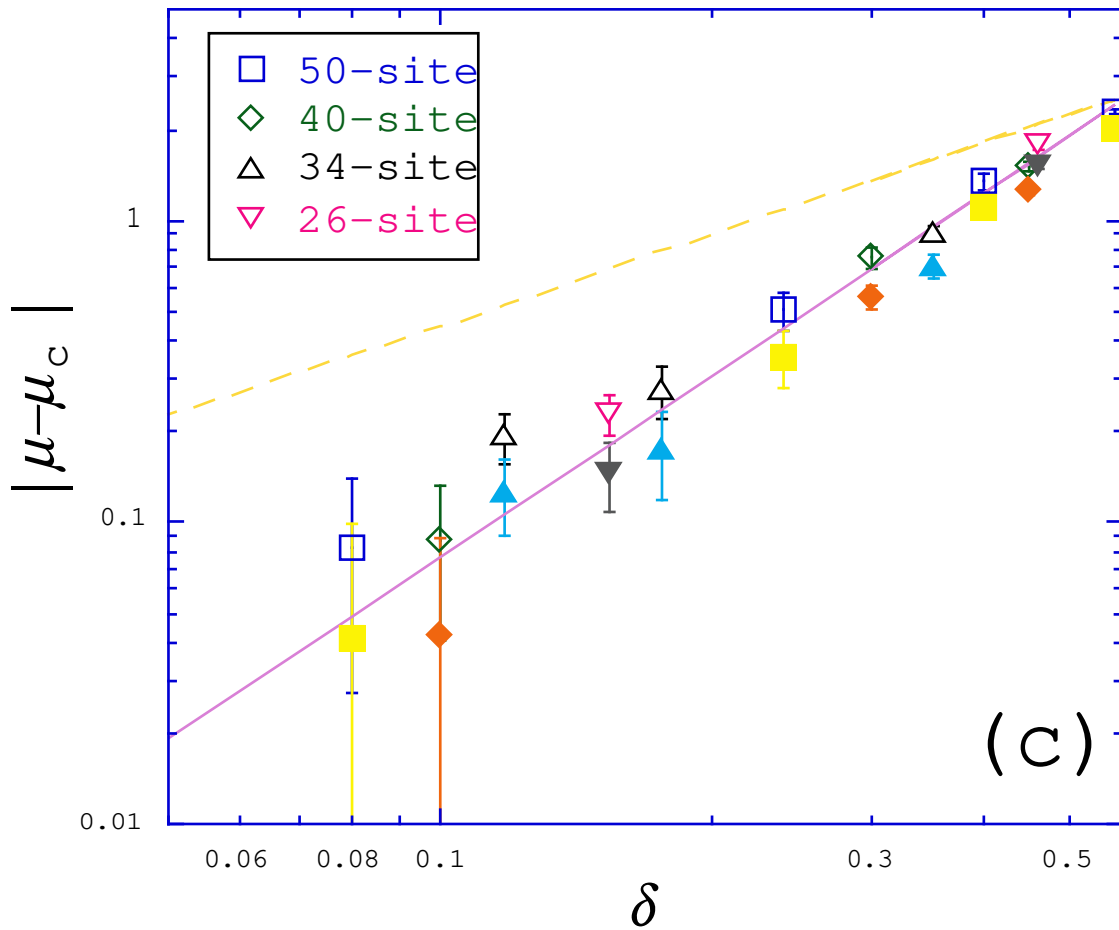


Fig. 10 (a) M. Kohno

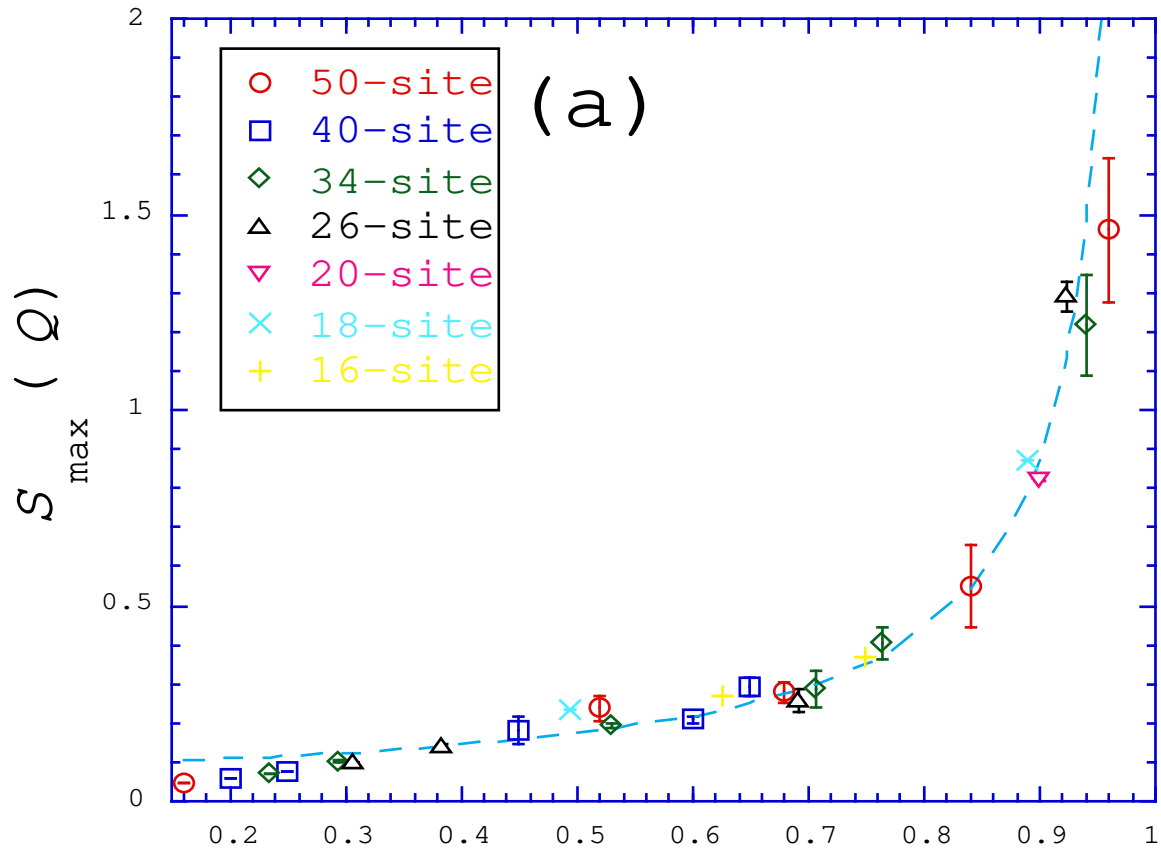


Fig. 10 (b) M. Kohnoⁿ

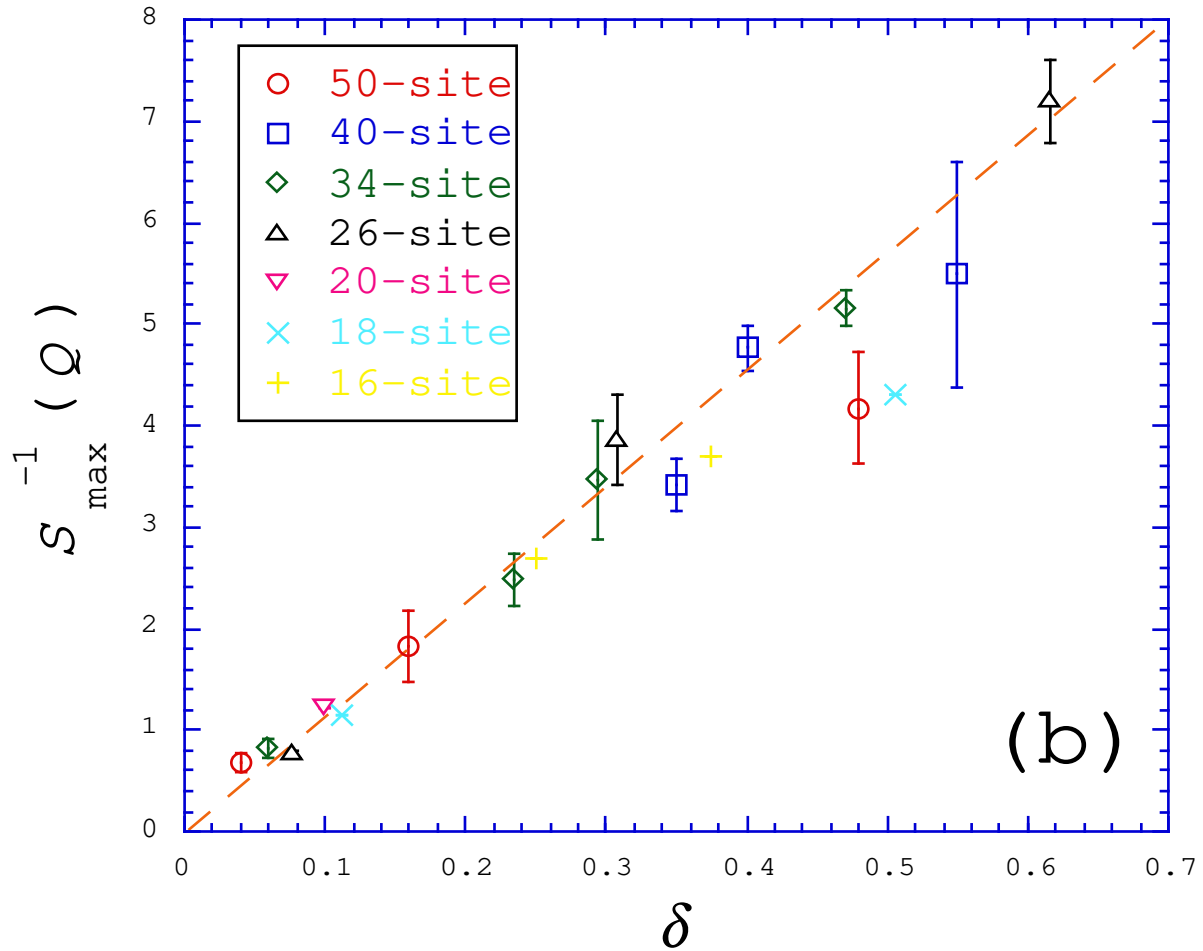


Fig.10 (c)

M.Kohno

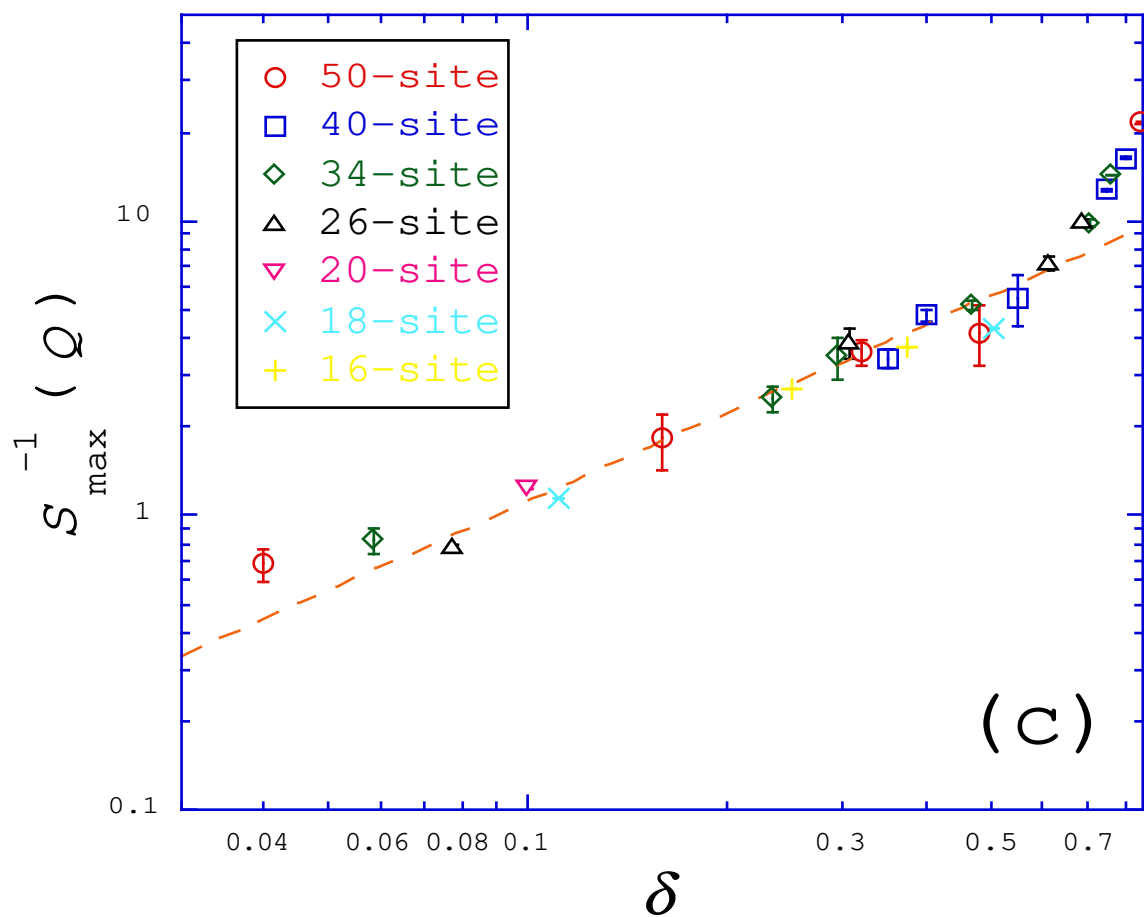


Fig.11 Inset

M.Kohno

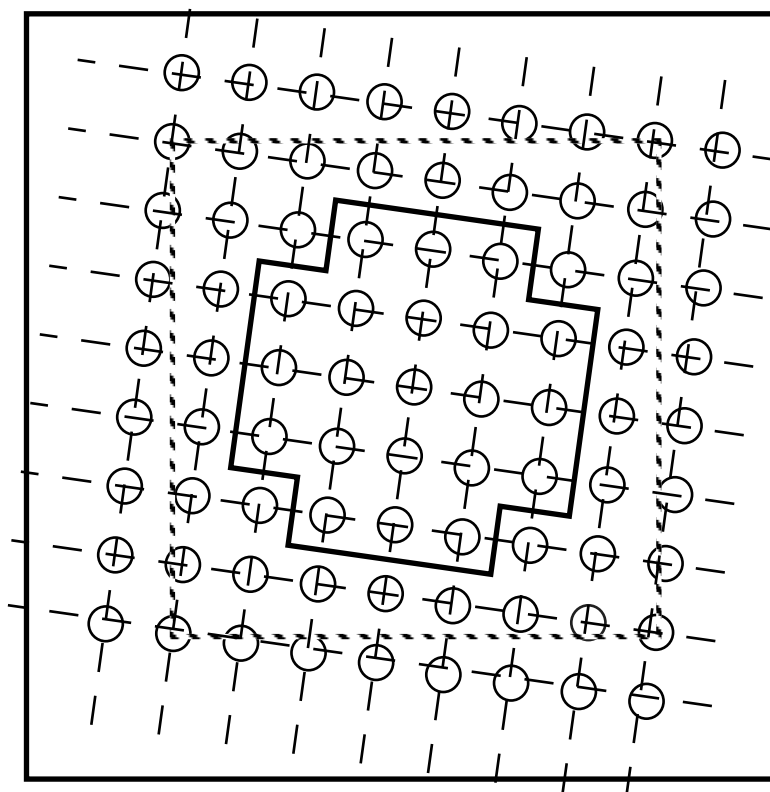


Fig.11 M.Kohno

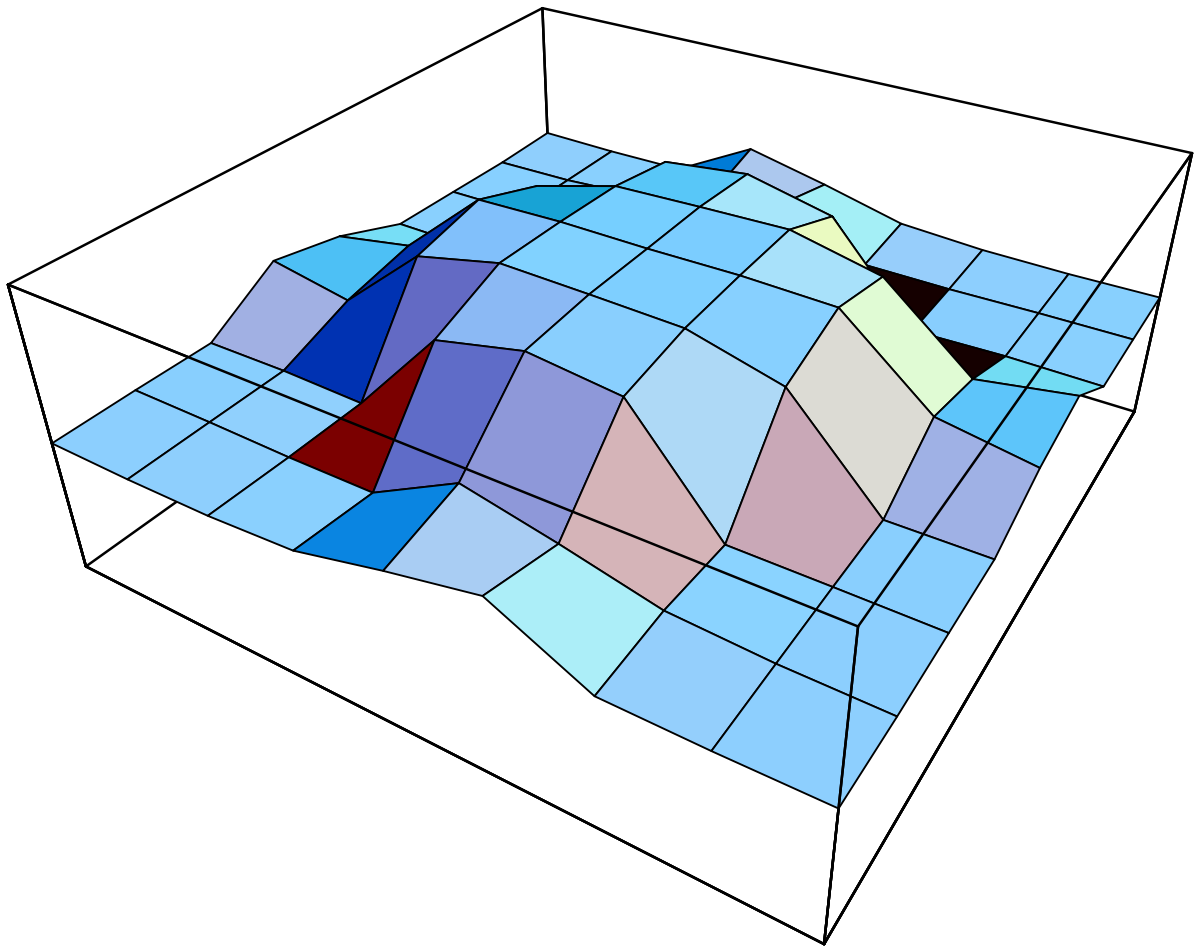


Fig. 5 M. Kohno

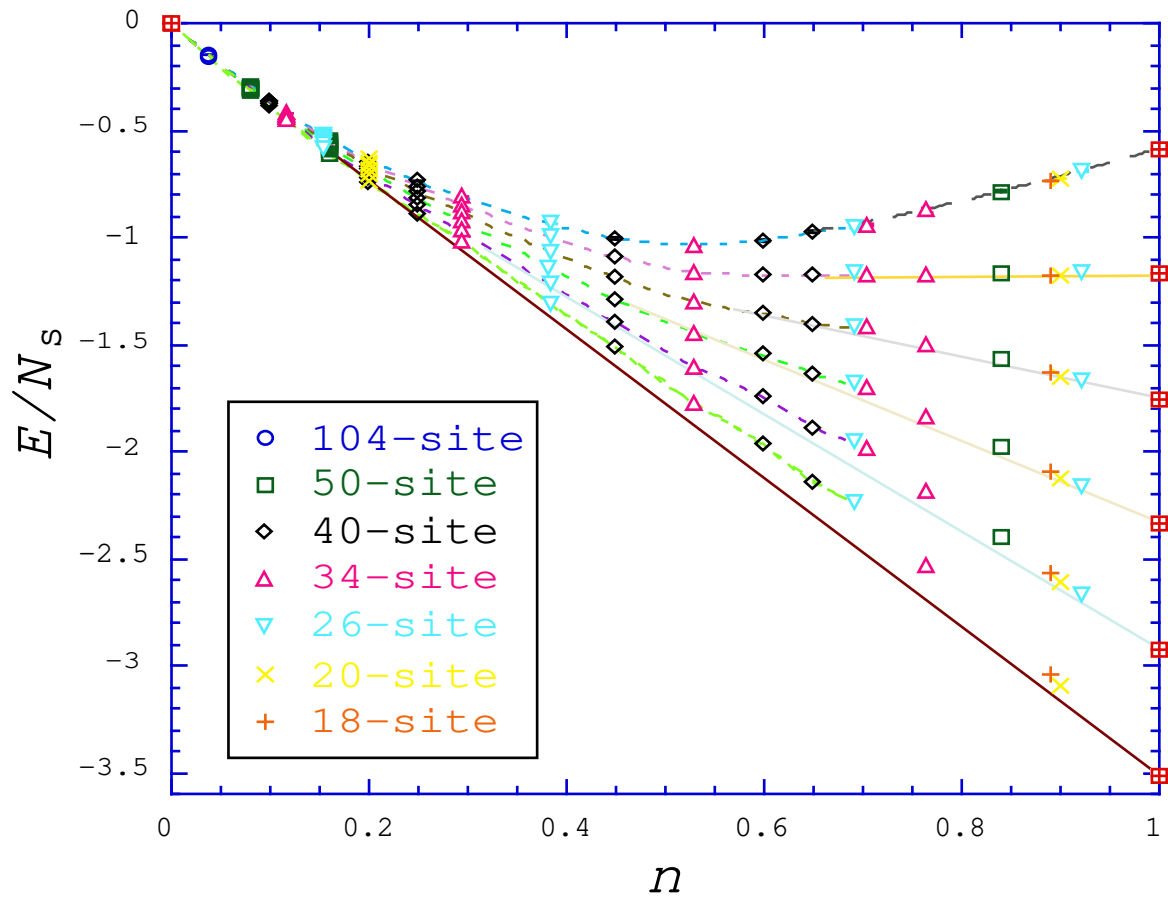


Fig. 12 M. Kohno

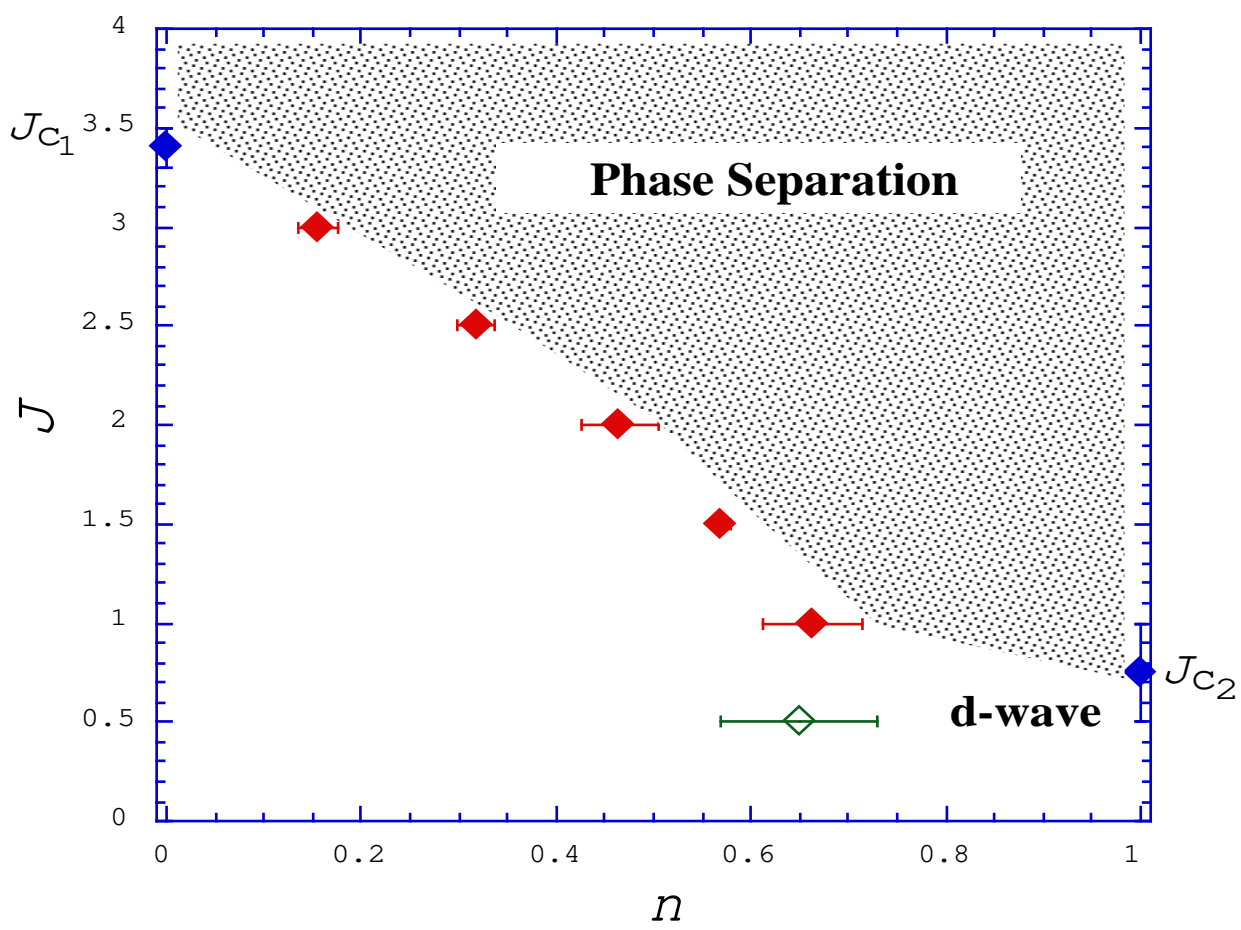


Fig.3 M.Kohno

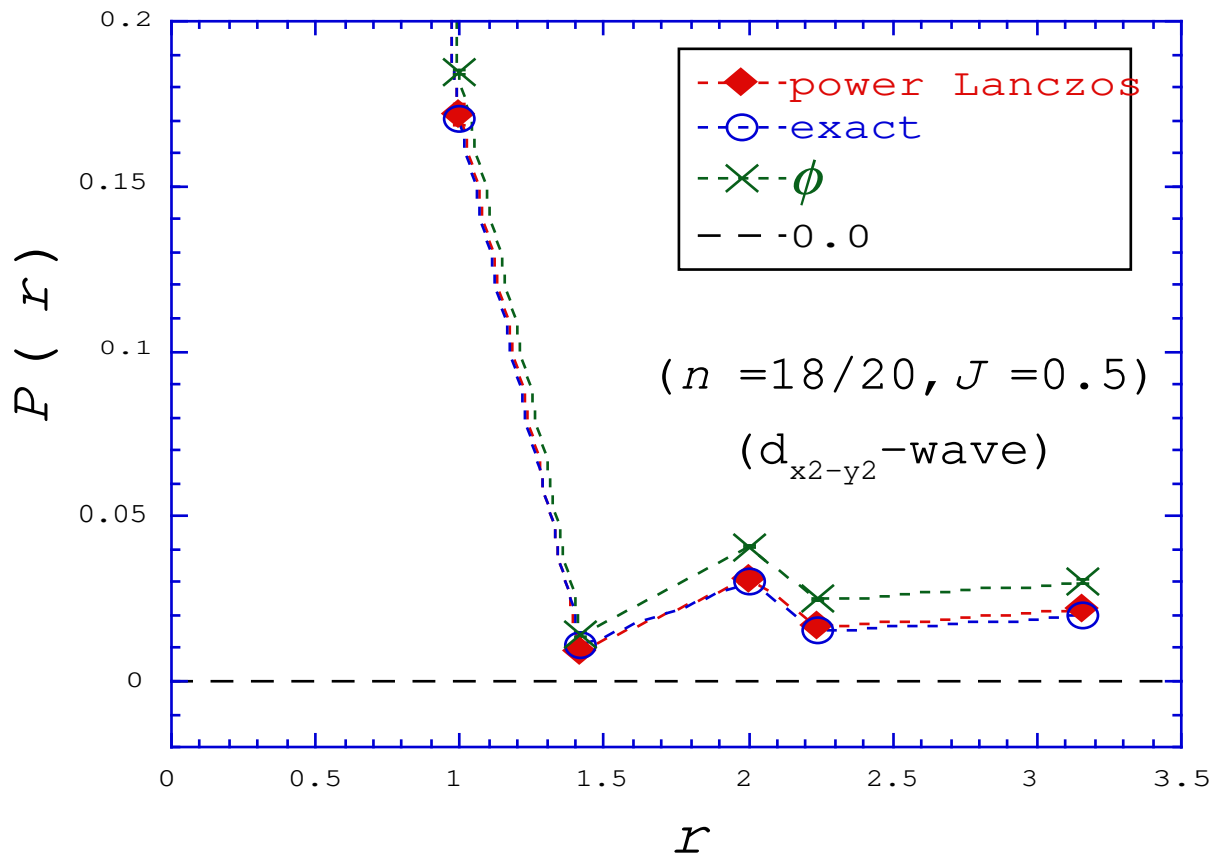


Fig.4 M.Kohno

